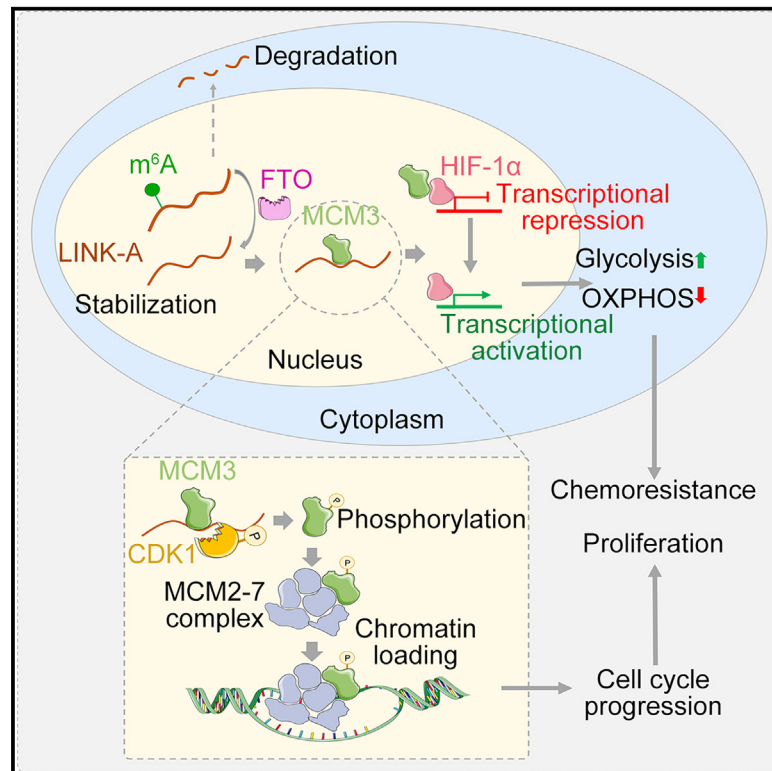


m⁶A demethylase FTO stabilizes LINK-A to exert oncogenic roles via MCM3-mediated cell-cycle progression and HIF-1 α activation

Graphical abstract



Authors

Yabing Nan, Shi Liu, Qingyu Luo, ..., Ruixiang Zhang, Yin Li, Zihua Liu

Correspondence

liyin@cicams.ac.cn (Y.L.), liuzh@cicams.ac.cn (Z.L.)

In brief

Nan et al. reveal that the m⁶A demethylase FTO stabilizes LINK-A to confer ESCC progression and chemoresistance. LINK-A directly interacts with MCM3, promoting CDK1-mediated MCM3 phosphorylation and subsequent cell-cycle progression, as well as disrupting MCM3-mediated HIF-1 α transcriptional suppression to trigger tumor glycolysis.

Highlights

- FTO demethylates and stabilizes LINK-A in an m⁶A-dependent manner
- LINK-A mediates MCM3 phosphorylation to facilitate cell-cycle progression
- LINK-A sequesters HIF-1 α from MCM3 to elicit its transcriptional activation
- Targeting LINK-A sensitizes ESCC to cytotoxic chemotherapy



Article

m⁶A demethylase FTO stabilizes LINK-A to exert oncogenic roles via MCM3-mediated cell-cycle progression and HIF-1 α activation

Yabing Nan,^{1,5} Shi Liu,^{1,5} Qingyu Luo,³ Xiaowei Wu,⁴ Pengfei Zhao,¹ Wan Chang,¹ Ruixiang Zhang,² Yin Li,^{2,*} and Zhihua Liu^{1,6,*}

¹State Key Laboratory of Molecular Oncology, National Cancer Center/National Clinical Research Center for Cancer/Cancer Hospital, Chinese Academy of Medical Sciences and Peking Union Medical College, Beijing 100021, China

²Department of Thoracic Surgery, National Cancer Center/National Clinical Research Center for Cancer/Cancer Hospital, Chinese Academy of Medical Sciences and Peking Union Medical College, Beijing 100021, China

³Department of Medical Oncology, Dana-Farber Cancer Institute, Harvard Medical School, Boston, MA 02215, USA

⁴Department of Cancer Biology, Dana-Farber Cancer Institute, Department of Genetics, Blavatnik Institute, Harvard Medical School, Boston, MA 02215, USA

⁵These authors contributed equally

⁶Lead contact

*Correspondence: liyin@cicams.ac.cn (Y.L.), liuzh@cicams.ac.cn (Z.L.)

<https://doi.org/10.1016/j.celrep.2023.113273>

SUMMARY

RNA N⁶-methyladenosine (m⁶A) modification is implicated in cancer progression, yet its role in regulating long noncoding RNAs during cancer progression remains unclear. Here, we report that the m⁶A demethylase fat mass and obesity-associated protein (FTO) stabilizes long intergenic noncoding RNA for kinase activation (LINK-A) to promote cell proliferation and chemoresistance in esophageal squamous cell carcinoma (ESCC). Mechanistically, LINK-A promotes the interaction between minichromosome maintenance complex component 3 (MCM3) and cyclin-dependent kinase 1 (CDK1), increasing MCM3 phosphorylation. This phosphorylation facilitates the loading of the MCM complex onto chromatin, which promotes cell-cycle progression and subsequent cell proliferation. Moreover, LINK-A disrupts the interaction between MCM3 and hypoxia-inducible factor 1 α (HIF-1 α), abrogating MCM3-mediated HIF-1 α transcriptional repression and promoting glycolysis and chemoresistance. These results elucidate the mechanism by which FTO-stabilized LINK-A plays oncogenic roles and identify the FTO/LINK-A/MCM3/HIF-1 α axis as a promising therapeutic target for ESCC.

INTRODUCTION

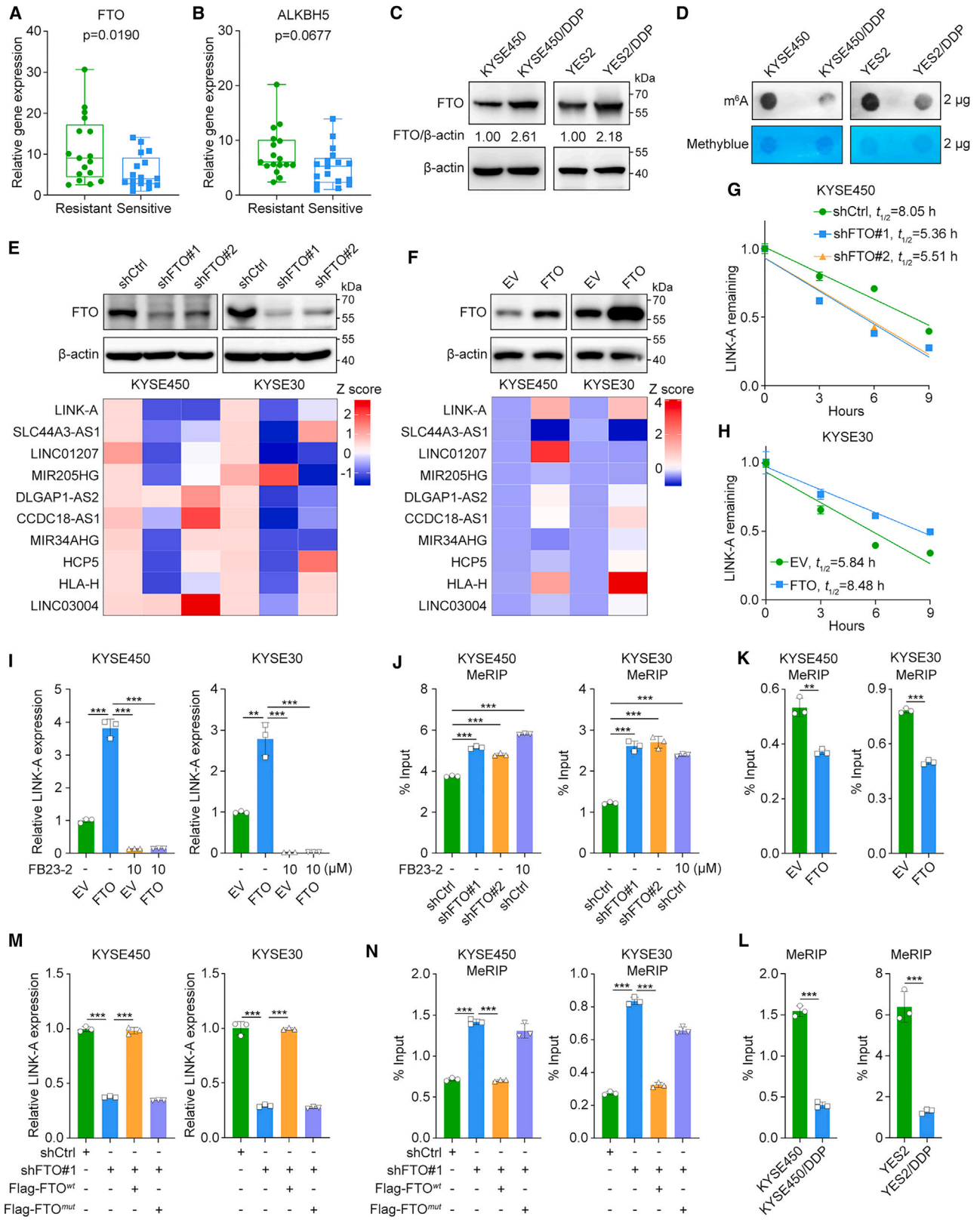
Esophageal cancer is a highly malignant tumor with the seventh highest incidence (approximately 604,000 new cases) and sixth highest mortality (approximately 544,000 deaths) worldwide in 2020.¹ The two main histologic subtypes of esophageal cancer, esophageal squamous cell carcinoma (ESCC) and esophageal adenocarcinoma, have distinct etiologies.² ESCC is the most common histologic subtype, with a poor prognosis and a high prevalence worldwide.² Chemotherapy is the first-line treatment for esophageal cancer, especially for patients with locally advanced cancer who have no indication for surgery. However, the benefits of chemotherapy are unsatisfactory, and the 5-year survival rate of patients with esophageal cancer is less than 20% because of chemoresistance.² Therefore, it is worthwhile to explore critical oncogenic drivers and elucidate the potential related molecular mechanisms to identify promising therapeutic targets for ESCC.

N⁶-methyladenosine (m⁶A) modification is the most abundant internal RNA modification in eukaryotes and occurs mainly in

mRNA.^{3,4} Accumulating evidence has shown that m⁶A modifications of noncoding RNAs (ncRNAs) such as microRNAs, long ncRNAs (lncRNAs), and circular RNAs also play essential roles in various physiological and pathological bioprocesses, including cancer development.^{5–7} m⁶A is installed by nuclear methyltransferases, termed “writers,” which are required for m⁶A deposition.^{4,8} m⁶A “reader” proteins, such as YTH domain-containing proteins and insulin-like growth factor-2 mRNA-binding proteins bind to m⁶A-containing RNAs to regulate their splicing, intracellular localization, and stability.^{9,10} m⁶A modification is dynamic and can be reversed by m⁶A demethylases, also called m⁶A “erasers,” including fat mass and obesity-associated protein (FTO) and α -ketoglutarate-dependent dioxygenase alkB homolog 5 (ALKBH5).^{11,12} Emerging evidence indicates that m⁶A modification can exert either oncogenic or tumor-suppressive effects in different contexts.^{13,14} However, the precise mechanism by which m⁶A modification regulates ncRNAs during cancer progression remains largely elusive.

The Warburg effect, a term that refers to the switch from oxidative phosphorylation (OXPHOS) to aerobic glycolysis, is a





(legend on next page)

well-known metabolic alteration in cancer cells.^{15–17} Although less efficient for ATP generation, aerobic glycolysis generates signaling metabolites to increase cancer cell survival and therapeutic resistance under stressful conditions.^{18,19} Hypoxia-inducible factor 1 (HIF-1), an oxygen-sensing transcription factor, controls whether glucose is metabolized via OXPHOS or glycolysis.²⁰ The oxygen-responsive HIF-1 α subunit and constitutively expressed HIF-1 β subunit interact to form the heterodimeric HIF-1 transcription factor, which plays critical roles in the cellular response to hypoxia.²¹ The accumulation of HIF-1 α and the HIF-1 α -mediated activation of glucose transporters and rate-limiting enzymes in glucose metabolism reduce the efficiency of OXPHOS and promote glycolysis.^{22–24} Although transcriptional activation of HIF-1 α has been reported to lead to cancer metabolic reprogramming and therapeutic resistance,²⁵ the mechanism by which lncRNAs regulate HIF-1 α activation in ESCC remains unclear.

Here, we found that the m⁶A demethylase FTO demethylates and stabilizes long intergenic ncRNA for kinase activation (LINK-A) in the context of ESCC chemoresistance. LINK-A directly interacts with minichromosome maintenance complex component 3 (MCM3) and cyclin-dependent kinase 1 (CDK1), and this interaction increases CDK1-mediated phosphorylation of MCM3 at Ser112 and facilitates the incorporation of MCM3 into the MCM2–7 complex and the subsequent chromatin loading of this complex, ultimately promoting cell-cycle progression. In contrast, LINK-A disrupts the interaction between MCM3 and HIF-1 α to free HIF-1 α and increase its transcriptional activity, which results in metabolic reprogramming from OXPHOS to glycolysis. Additionally, targeting LINK-A substantially sensitizes patient-derived xenografts (PDXs) to first-line chemotherapy, indicating that LINK-A may be a potential target for cancer treatment.

RESULTS

FTO stabilizes LINK-A and correlates with chemoresistance

To study the m⁶A modification of critical lncRNAs in the context of ESCC chemoresistance, we collected 34 baseline samples from patients with ESCC who received neoadjuvant chemo-

therapy (17 chemoresistant and 17 chemosensitive) and then measured the mRNA expression levels of two dominant m⁶A demethylases, FTO and ALKBH5.²⁶ The results of real-time qPCR indicated that FTO, but not ALKBH5, was significantly upregulated in chemoresistant samples compared with chemosensitive samples (Figures 1A and 1B). Furthermore, we measured the protein level of FTO in previously established parental and chemoresistant ESCC cell lines.²⁷ FTO protein expression was upregulated in both chemoresistant cell lines compared with the corresponding parental cells (Figure 1C). Consistent with the upregulated FTO expression in chemoresistant cells, the results of the m⁶A dot blot assay showed that the overall level of m⁶A was decreased in the chemoresistant cells compared with the parental cells (Figure 1D). Subsequently, to further identify FTO-regulated lncRNAs, we silenced and overexpressed FTO in two ESCC cell lines and then measured the expression levels of 14 annotated ncRNAs previously shown to be significantly upregulated in chemoresistant ESCC cell lines compared with the corresponding parental cell lines.²⁷ The expression of four ncRNAs (TTLL3, LINC00663, PRSS30P, and CETN4P) was below the detection limit of real-time qPCR. Among the remaining 10 ncRNAs, only LINK-A was significantly downregulated after FTO knockdown and upregulated after FTO overexpression in both KYSE30 and KYSE450 cells (Figures 1E and 1F). Additionally, correlation analyses showed that LINK-A expression was positively correlated with the FTO mRNA level, but only weakly correlated with the ALKBH5 mRNA expression level in the ESCC dataset (Figures S1A and S1B).

To specify the mechanism by which FTO modulates LINK-A expression in the context of ESCC chemoresistance, we first sought to determine whether FTO affects LINK-A biosynthesis. No significant change in LINK-Aⁿ RNA biosynthesis was observed in either KYSE450 or KYSE30 cells with FTO depletion (Figure S1C). Next, we performed an RNA stability assay and found that knockdown of FTO dramatically shortened the half-life of LINK-A and that overexpression of FTO stabilized LINK-A (Figures 1G and 1H). Subsequently, we treated control and FTO-overexpressing KYSE30 and KYSE450 cells with the FTO inhibitor FB23-2. Overexpression of FTO markedly increased the expression level of LINK-A, whereas treatment

Figure 1. FTO stabilizes LINK-A and correlates with chemoresistance

(A and B) Real-time qPCR analysis of mRNA expression for FTO (A) and ALKBH5 (B) in baseline samples obtained from patients with ESCC categorized into chemosensitive and chemoresistant groups. Boxplot representation: from top to bottom—maximum, 75th percentile, median, 25th percentile and minimum values; unpaired Student's t test; n = 17 for chemoresistant patients and n = 17 for chemosensitive patients.

(C) Western blot analysis of FTO protein expression in chemoresistant and parental ESCC cell lines.

(D) Total m⁶A levels in chemoresistant and parental ESCC cell lines, as determined by an m⁶A dot blot assay. Methylene blue staining was used to verify equal loading.

(E and F) Western blot and heatmap of real-time qPCR data in the indicated cells.

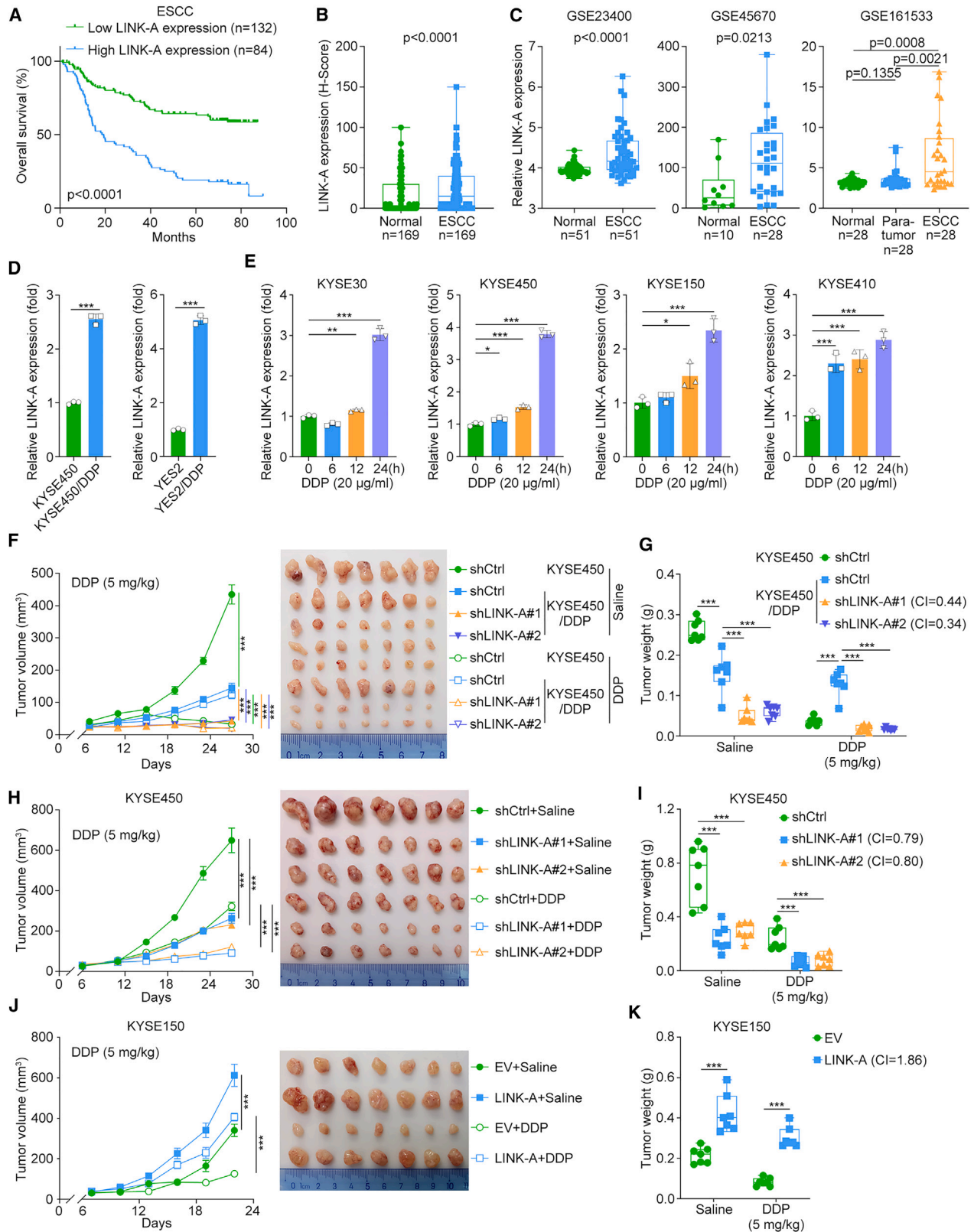
(G and H) Kinetic analysis of RNA stability in the indicated cells. Actinomycin D (5 μ g/mL) was added at time 0. The data are presented as the mean \pm SD values; n = 3.

(I) Real-time qPCR analysis of LINK-A expression in the indicated cells. Cells were pretreated with FB23-2 for 24 h. The data are presented as the mean \pm SD values; unpaired Student's t test, **p < 0.01, ***p < 0.001; n = 3.

(J–L) MeRIP-qPCR analysis of LINK-A m⁶A modification in the indicated cells. Control cells were pretreated with FB23-2 for 24 h in (J). The data are presented as the mean \pm SD values; unpaired Student's t test, **p < 0.01, ***p < 0.001; n = 3.

(M) Real-time qPCR analysis of LINK-A expression in the indicated cells. The data are presented as the mean \pm SD values; unpaired Student's t test, ***p < 0.001; n = 3.

(N) MeRIP-qPCR analysis of LINK-A m⁶A modification in the indicated cells. The data are presented as the mean \pm SD values; unpaired Student's t test, ***p < 0.001; n = 3.



(legend on next page)

with FB23-2 abrogated this effect (Figure 1I). In addition, we determined whether the stabilization of LINK-A by FTO is dependent on its demethylase activity. The methylated RNA immunoprecipitation (MeRIP)-qPCR results indicated that both knockdown of FTO and treatment with FB23-2 significantly increased, but overexpression of FTO decreased, the m⁶A level of LINK-A (Figures 1J and 1K). Consistent with this finding, the MeRIP-qPCR results showed that the m⁶A level of LINK-A was significantly decreased in chemoresistant cells compared with parental cells (Figure 1L). Finally, we performed rescue assays using both wild-type FTO and an FTO mutant harboring two point mutations, H231A and D233A,¹² which are known to impede the enzymatic function of FTO (Figure S1D). The real-time qPCR results indicated that wild-type but not mutated FTO reversed the decreased LINK-A expression caused by FTO knockdown in both KYSE30 and KYSE450 cells (Figure 1M). Furthermore, the results of MeRIP-qPCR showed that transduction of wild-type FTO led to a significant decrease in the LINK-A methylation levels in FTO-silenced KYSE30 and KYSE450 cells, whereas this demethylation did not occur after transduction of the FTO mutant (Figure 1N). These results demonstrate that FTO stabilizes LINK-A expression in an m⁶A-dependent manner.

LINK-A exerts oncogenic roles in ESCC

To investigate the roles of LINK-A in ESCC, we analyzed LINK-A expression in a cohort of patients with ESCC by performing *in situ* hybridization. Survival analysis indicated that high LINK-A expression was strongly correlated with a poor prognosis (Figure 2A). In addition, LINK-A expression in cancer tissues was significantly higher than that in normal tissues (Figure 2B). However, LINK-A expression was not significantly correlated with any other clinicopathological feature, except for lymph node metastasis (Figure S2A). Moreover, the significant upregulation of LINK-A in cancer tissues was validated in the GEO database (Figure 2C). To further evaluate the potential of LINK-A as a therapeutic target for ESCC, we used an *in vitro* model of chemoresistance. We measured the LINK-A expression level in ESCC cells with long-term induction of chemoresistance (KYSE450/DDP and YES2/DDP) and the corresponding parental cells (KYSE450 and YES2) and found that the expression of LINK-A was dramatically upregulated (2- to 5-fold) in the chemoresistant cells compared with the parental cells (Figure 2D). To determine the alteration of LINK-A in the response to short-term drug expo-

sure, we treated ESCC cells with cisplatin (DDP) for different durations (0, 6, 12, and 24 h). LINK-A expression increased significantly with increasing DDP treatment time, especially after treatment for 24 h (Figure 2E). These results suggest that LINK-A may exert crucial roles in both the acquisition and maintenance of chemoresistance.

Next, to verify the oncogenic roles of LINK-A, we performed *in vitro* and *in vivo* loss- and gain-of-function experiments. First, we overexpressed LINK-A in the normal esophageal epithelial cell line Het-1A and then performed cell proliferation assays (Figure S2B). Overexpression of LINK-A significantly facilitated the proliferation of Het-1A cells (Figure S2C). Next, we measured the expression of LINK-A in a panel of ESCC cell lines and selected KYSE450 cells, with relatively high LINK-A expression, for LINK-A silencing and KYSE150 and KYSE410 cells, with relatively low LINK-A expression, for LINK-A overexpression (Figures S2D–S2F). We also established chemoresistant ESCC cell lines with stable LINK-A silencing (Figure S2E). IncuCyte live cell imaging analysis showed that silencing LINK-A significantly inhibited cell proliferation in both the chemoresistant and parental ESCC cell lines, whereas overexpression of LINK-A promoted cell proliferation (Figures S2G–S2I). Subsequently, the results of the cell viability assay indicated that silencing LINK-A increased the sensitivity of both the chemoresistant and parental ESCC cells to cytotoxic chemotherapy, while overexpression of LINK-A promoted chemoresistance (Figures S2J–S2L). Finally, the xenograft assays indicated that silencing LINK-A in KYSE450/DDP and KYSE450 cells dramatically retarded tumor growth and elicited chemosensitivity, while overexpression of LINK-A in KYSE150 cells significantly promoted tumor growth and resistance to cytotoxic chemotherapy (Figures 2F–2K). Taken together, these results indicate that LINK-A plays oncogenic roles in ESCC.

LINK-A facilitates MCM3 phosphorylation by promoting the interaction between MCM3 and CDK1

To further delineate the downstream regulatory mechanism underlying the oncogenic roles of LINK-A, we performed mass spectrometry analyses to identify proteins precipitated by LINK-A in KYSE450 and YES2 cells. In total, 43 and 14 LINK-A-interacting proteins were identified in KYSE450 and YES2 cells, respectively, and 7 of these interacting proteins were identified in both cell lines (Figure 3A). Among these seven

Figure 2. LINK-A exerts oncogenic roles in ESCC

- (A) Overall survival of patients with ESCC stratified by LINK-A expression levels (low and high, based on the mean expression level) is depicted in Kaplan-Meier survival curves.
- (B) Statistical analysis of LINK-A expression in 169 paired ESCC tissues and adjacent normal tissues. Boxplot representation: from top to bottom—maximum, 75th percentile, median, 25th percentile and minimum values; paired Student's t test.
- (C) Statistical analysis of LINK-A expression in ESCC tissues and adjacent normal tissues from the GEO database. Boxplot representation: from top to bottom—maximum, 75th percentile, median, 25th percentile and minimum values; unpaired Student's t test in GSE45670 and paired Student's t test in GSE23400 and GSE161533.
- (D) Real-time qPCR analysis of LINK-A expression in the indicated cells. The data are presented as the mean \pm SD values; unpaired Student's t test, ***p < 0.001; n = 3.
- (E) Real-time qPCR analysis of LINK-A expression in the indicated cells treated with DDP for 0, 6, 12, and 24 h. The data are presented as the mean \pm SD values; unpaired Student's t test, *p < 0.05, **p < 0.01, ***p < 0.001; n = 3.
- (F–K) Growth curves and representative images (F, H, and J) and weights (G, I, and K) of the xenograft tumors derived from the indicated cells. The data are presented as the mean \pm SEM. values in (F, H, and J). Boxplot representation: from top to bottom—maximum, 75th percentile, median, 25th percentile and minimum values in (G), (I) and (K); unpaired Student's t test, ***p < 0.001; n = 7.

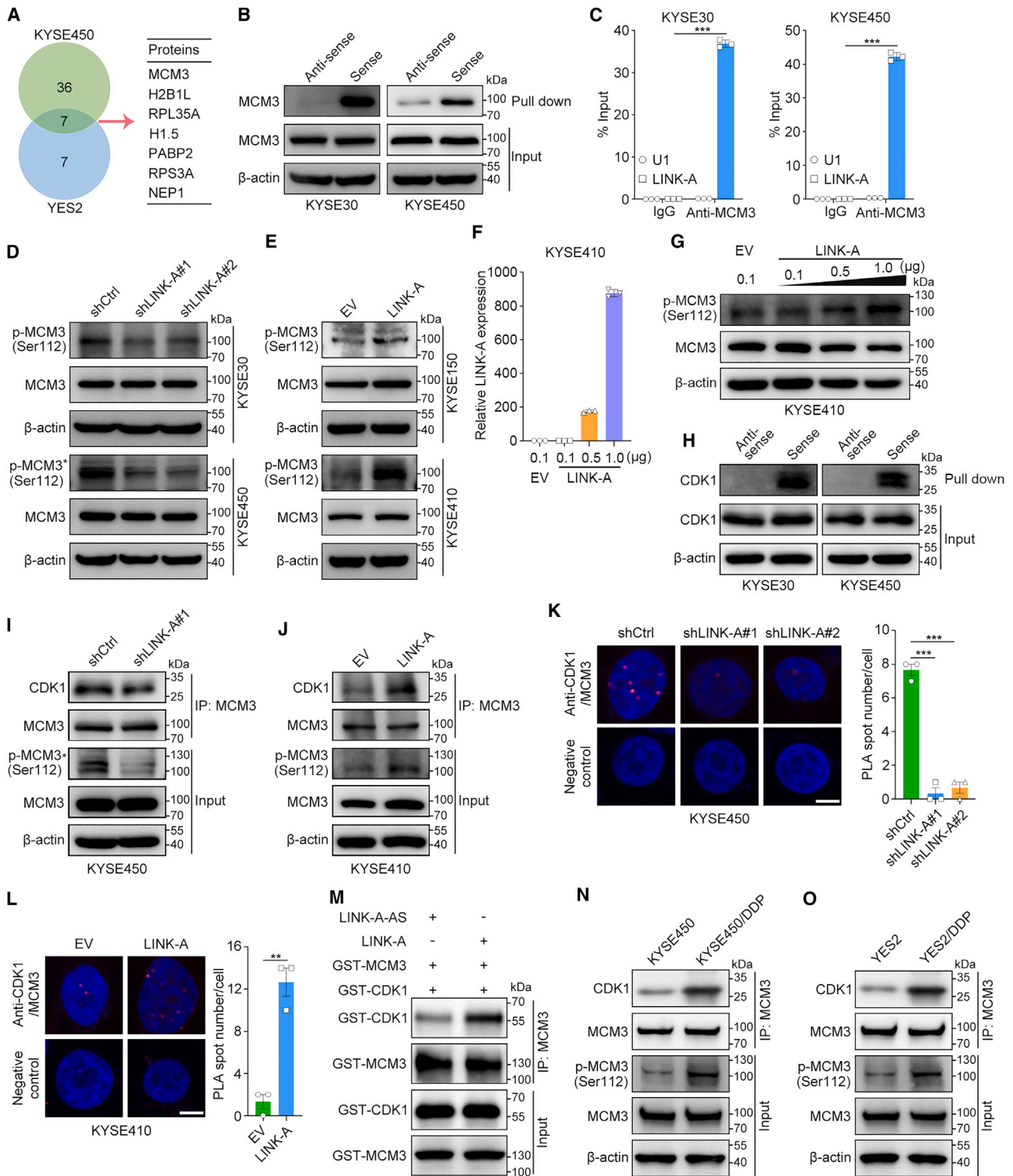


Figure 3. LINK-A facilitates MCM3 phosphorylation by promoting the interaction between MCM3 and CDK1

(A) List of LINK-A-associated proteins identified by MS following RNA pull-down in KYSE450 and YES2 cells.

(B) Western blot analysis of MCM3 expression following RNA pull-down in the indicated cells.

(C) Real-time qPCR analysis of LINK-A and U1 expression following RIP assays in the indicated cells. The data are presented as the mean \pm SD values; unpaired Student's t test, *** $p < 0.001$; $n = 3$.

(legend continued on next page)

overlapping proteins, MCM3 has been reported to play an important role in cell-cycle progression and DNA replication,²⁸ whereas its detailed molecular mechanisms in ESCC, especially in mediating cancer cell proliferation and chemoresistance, remain elusive. Next, we performed RNA pull-down followed by western blotting to confirm the specific interaction between MCM3 and LINK-A sense strand, but not antisense strand (Figure 3B). Moreover, this interaction was validated in KYSE30 and KYSE450 cells by RIP-qPCR (Figure 3C). Subsequently, the nuclear localization of LINK-A and the signal specificity of the LINK-A probe in control and LINK-A-silenced ESCC cells were confirmed by fluorescence *in situ* hybridization (FISH) (Figures S3A and S3B). Furthermore, the results of FISH and immunofluorescence (IF) double staining showed that endogenous LINK-A and MCM3 colocalized in the nucleus (Figure S3C). Next, we explored the effect of LINK-A on the expression of its interacting protein MCM3. Neither knockdown nor overexpression of LINK-A affected the mRNA or protein level of MCM3 (Figures 3D, 3E, S3D, and S3E). Strikingly, western blot analysis indicated that LINK-A markedly facilitated MCM3 phosphorylation at Ser112 (Figures 3D and 3E). Moreover, the level of MCM3 phosphorylation at Ser112 was increased in a dose-dependent manner upon transient LINK-A overexpression (Figures 3F and 3G).

A previous study reported that CDK1 phosphorylates MCM3 at Ser112 and mediates the assembly and chromatin loading of MCM2-7 complex.²⁹ We then determined whether LINK-A promotes MCM3 phosphorylation by acting as a scaffold for CDK1 and MCM3. The results of RNA pull-down followed by western blotting confirmed the interaction between LINK-A and CDK1 in KYSE30 and KYSE450 cells (Figure 3H). In addition, the results of FISH and IF double staining indicated colocalization of endogenous LINK-A and CDK1 in the nucleus (Figure S3F). Next, the results of co-immunoprecipitation (coIP) assay indicated that knockdown of LINK-A dramatically suppressed and overexpression of LINK-A increased the interaction between CDK1 and MCM3 (Figures 3I and 3J). The proximity ligation assay results confirmed that LINK-A promoted the interaction between CDK1 and MCM3 *in vivo* (Figures 3K and 3L). In addition, we performed *in vitro* pull-down assays using purified MCM3 and CDK1 proteins in buffer containing the LINK-A sense or antisense strand. The results demonstrated that the presence of the LINK-A sense strand, but not the antisense strand, promoted the *in vitro* interaction between MCM3 and CDK1 (Figure 3M). Consistent with this finding, the phosphorylation of MCM3 at Ser112 and the interaction between CDK1 and MCM3 were increased in both chemoresistant cell lines compared with the corresponding parental cell lines (Figures 3N and 3O).

Phosphorylated MCM3 mediates the oncogenic roles of LINK-A

To determine whether LINK-A-mediated MCM3 phosphorylation promotes the assembly and subsequent chromatin loading of the MCM complex, we performed cellular fractionation and then detected chromatin-bound proteins by western blot analysis. Knockdown of LINK-A dramatically decreased the chromatin loading of MCM2, MCM3, MCM4, MCM5, MCM6, and MCM7 proteins, whereas overexpression of LINK-A promoted chromatin loading of the MCM2-7 complex in ESCC cells (Figures 4A and 4B). Next, we constructed a Ser112 site mutant of MCM3 (MCM3^{S112A}; Ser112 mutated to alanine) and transfected wild-type MCM3 and MCM3^{S112A} into cells with depletion of endogenous MCM3 (Figure S4A). The increased chromatin loading of the MCM2-7 complex mediated by LINK-A was abolished by mutation of Ser112, indicating that this process depends on MCM3 phosphorylation (Figure 4C). To determine whether MCM3 mediates the promoting effect of LINK-A on cell-cycle progression, we performed rescue assays and found that overexpression of wild-type MCM3 but not MCM3^{S112A} completely rescued LINK-A silencing-mediated G0/G1 arrest (Figures 4D, S4B, and S4C). In contrast, silencing MCM3 in LINK-A-overexpressing KYSE410 cells abolished LINK-A-mediated cell-cycle progression (Figures 4E, S4D, and S4E). Furthermore, IncuCyte live cell imaging analysis indicated that wild-type MCM3 but not MCM3^{S112A} mediated the promoting effect of LINK-A on cell proliferation (Figures 4F and 4G). To further demonstrate the functional relationship between MCM3 and LINK-A *in vivo*, we performed xenograft assay with KYSE150 cells (Figure S4F). Overexpression of LINK-A markedly promoted cell proliferation and chemoresistance, whereas silencing of MCM3 abrogated these effects (Figures 4H and 4I). Taken together, these results indicate that LINK-A exerts oncogenic effects by increasing MCM3 phosphorylation to facilitate the assembly and subsequent chromatin loading of the MCM2-7 complex.

LINK-A elicits HIF-1 α transcriptional activity by sequestering HIF-1 α from MCM3

To further study the mechanism by which the LINK-A/MCM3 axis leads to resistance to cytotoxic chemotherapy, we performed RNA sequencing analysis in LINK-A-silenced KYSE450 cells. Strikingly, gene set enrichment analysis showed that the glycolysis pathway was significantly enriched in control cells compared with cells with LINK-A knockdown mediated by either of two independent short hairpin RNA sequences (Figure 5A). Given the observation in a previous study that MCM3 negatively regulates HIF-1 α transcriptional activity by directly interacting

(D and E) Western blot analysis of MCM3 and phosphorylated MCM3 protein levels in the indicated cells. *Nonspecific band.

(F and G) Real-time qPCR analysis of LINK-A expression (F) and western blot analysis of MCM3 and phosphorylated MCM3 protein levels (G) after exogenous expression of increasing amounts of LINK-A in KYSE410 cells.

(H) Western blot analysis of CDK1 expression following RNA pull-down in the indicated cells.

(I and J) Western blot analysis of the interaction between MCM3 and CDK1 following coIP assays in the indicated cells. *Nonspecific band.

(K and L) Representative images of the merged proximity ligation assay (PLA) and nuclear (DAPI) channels and quantitative analysis of PLA puncta in the indicated cells. The scale bar represents 10 μ m. The data are presented as the mean \pm SEM. values; unpaired Student's t test, **p < 0.01, ***p < 0.001; n = 3.

(M) Western blot analysis of the interaction between MCM3 and CDK1 *in vitro*.

(N and O) Western blot analysis of the interaction between MCM3 and CDK1 after coIP assays in the indicated cells.

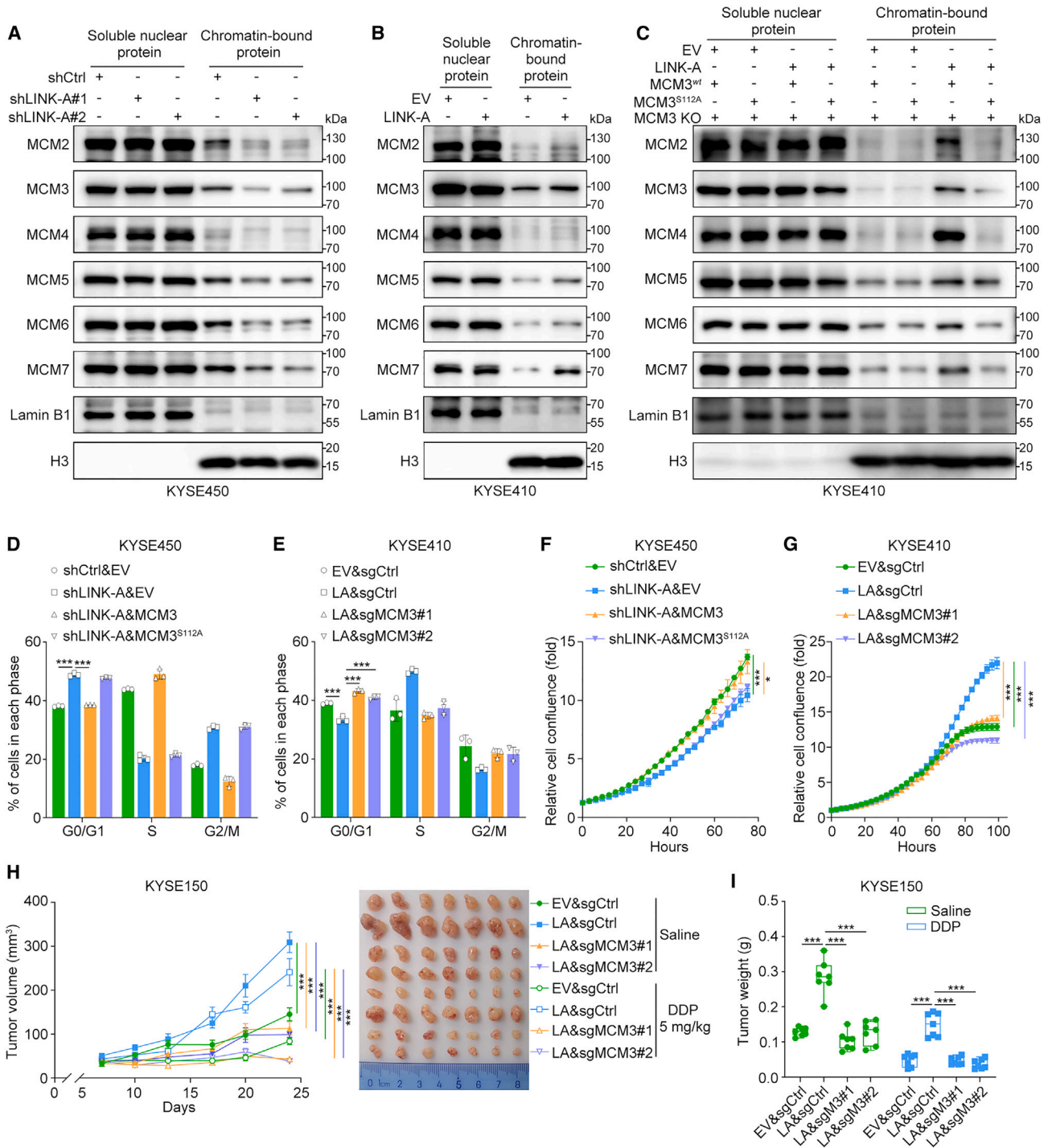


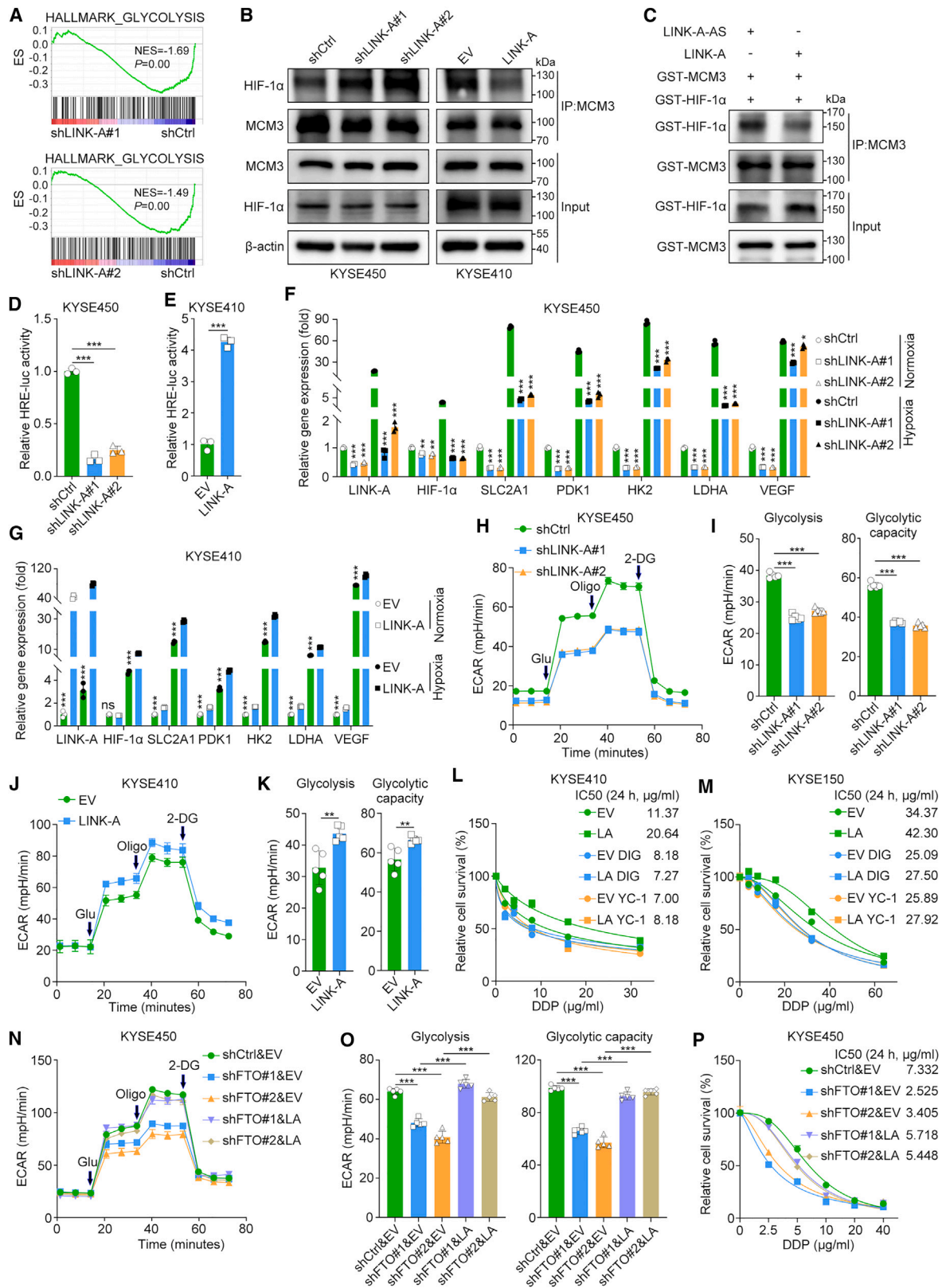
Figure 4. Phosphorylated MCM3 mediates the oncogenic roles of LINK-A

(A–C) Western blot analysis of the nuclear and chromatin-bound proteins in the indicated cells.

(D and E) Quantitative analysis of the cell-cycle distribution (percentages) in the indicated cells. The data are presented as the mean \pm SD values; unpaired Student's t test, *** p < 0.001; n = 3.

(F and G) IncuCyte live cell imaging analysis of the indicated cells. The data are presented as the mean \pm SD values; unpaired Student's t test, * p < 0.05, *** p < 0.001; n = 3.

(H and I) Volumes and representative images (H) and weights (I) of the xenograft tumors derived from the indicated cells. The data are presented as the mean \pm SEM. values in (H). Boxplot representation: from top to bottom—maximum, 75th percentile, median, 25th percentile and minimum values in (I); unpaired Student's t test, *** p < 0.001; n = 7.



(legend on next page)

with HIF-1 α ,³⁰ we sought to determine whether LINK-A activates HIF-1 α to promote tumor glycolysis. First, we determined whether LINK-A influences the interaction between MCM3 and HIF-1 α by performing IP assays in LINK-A-silenced KYSE450 cells and LINK-A-overexpressing KYSE410 cells under normoxic conditions. The results suggested that silencing LINK-A markedly increased, but overexpressing LINK-A, suppressed the interaction between MCM3 and HIF-1 α (Figure 5B). Consistent with this finding, the inhibitory effect of LINK-A on the interaction between MCM3 and HIF-1 α was also confirmed under hypoxic conditions (Figure S5A). Moreover, we purified MCM3 and HIF-1 α proteins by GST pull-down and then performed *in vitro* coIP assays in buffer containing the LINK-A sense or antisense strand. The presence of the LINK-A sense strand but not the antisense strand suppressed the interaction between MCM3 and HIF-1 α *in vitro* (Figure 5C). Since the protein level of HIF-1 α was not altered by either overexpression or knockdown of LINK-A (Figures S5B and S5C), we hypothesized that LINK-A may regulate transcriptional activity of HIF-1 α . Consistent with this hypothesis, silencing LINK-A markedly suppressed and overexpression of LINK-A enhanced hypoxia response element-driven luciferase activity (Figures 5D and 5E). Moreover, the real-time qPCR results indicated that LINK-A dramatically facilitated the expression of HIF-1 α target genes, including SLC2A1, PDK1, HK2, LDHA, and vascular endothelial growth factor, under both normoxic and hypoxic conditions (Figures 5F and 5G). Notably, the expression of LINK-A and HIF-1 α target genes was significantly upregulated under hypoxic conditions compared with normoxic conditions (Figures 5F and 5G), further confirming the functional correlation between LINK-A and HIF-1 α transcriptional activity.

Given the important roles of HIF-1 α in cancer metabolic reprogramming, we performed Seahorse assays to determine the effect of LINK-A on tumor glycolysis. Knockdown of LINK-A significantly decreased the extracellular acidification rate (ECAR), but moderately increased the oxygen consumption rate (OCR) (Figures 5H, 5I, S5D, and S5E). Similarly, overexpression of LINK-A increased the ECAR, but decreased the OCR (Figures 5J, 5K, S5F, and S5G). Subsequently, a significant increase in glycolytic activity was detected in both chemoresistant cell lines compared with parental cell lines (Figures S5H–S5K). Furthermore, we examined whether HIF-1 α mediates the role of LINK-A in chemoresistance of ESCC. The results of cell viability assay showed that treatment with the HIF-1 α inhibitors

licifiguat (YC-1) and digoxin markedly suppressed the oncogenic effects of LINK-A in KYSE410 and KYSE150 cells (Figures 5L and 5M). Taken together, these results suggest that LINK-A activates HIF-1 α by abrogating the MCM3-mediated transcriptional repression of HIF-1 α and then facilitates glycolysis and chemoresistance. Finally, to further confirm the involvement of FTO in LINK-A/MCM3/HIF-1 α -mediated glycolysis and chemoresistance, we performed functional rescue experiments in KYSE450 cells (Figures S5L and S5M). The results of the Seahorse assays revealed a significant reduction in glycolytic activity upon FTO knockdown, with subsequent reversal of this decrease observed upon overexpression of LINK-A (Figures 5N and 5O). Consistent with this finding, overexpression of LINK-A in FTO-silenced cells restored the phenotype of decreased proliferation and decreased chemoresistance (Figures 5P and S5N).

Having demonstrated that the interaction between LINK-A and MCM3 transcriptionally activates HIF-1 α and promotes MCM3 phosphorylation at Ser112 and subsequent cell-cycle progression (Figure S6A), we sought to determine whether phosphorylation of MCM3 at Ser112 regulates the interaction between MCM3 and HIF-1 α . The results of coIP assays indicated that the modulation of MCM3-HIF-1 α interaction by LINK-A was not affected by MCM3^{S112A} mutation (Figures S6B and S6C). Moreover, we treated control and LINK-A-overexpressing cells with HIF-1 α inhibitors and then analyzed the cell-cycle distribution. Although treatment with either HIF-1 α inhibitor led to G0/G1 arrest, LINK-A-mediated cell-cycle progression was not affected by HIF-1 α inhibitor treatment (Figures S6D–S6G). Taken together, these results indicate that the effects of the LINK-A/MCM3 axis on HIF-1 α transcriptional activation and MCM3 phosphorylation-dependent cell-cycle progression are independent.

Targeting LINK-A sensitizes ESCC to cytotoxic chemotherapy

To determine whether targeting LINK-A is a promising therapeutic strategy for ESCC, we established three PDX models. Adeno-associated virus-mediated silencing of LINK-A dramatically increased DDP sensitivity in ESCC PDXs (Figures 6A–6F). Finally, we measured the transcript level of LINK-A in the same baseline samples shown in Figure 1A. The results indicated that the expression level of LINK-A was significantly upregulated in the chemoresistant samples compared with the chemosensitive

Figure 5. LINK-A induces HIF-1 α transcriptional activation by sequestering HIF-1 α from MCM3

- (A) Enriched pathways identified by gene set enrichment analysis based on RNA sequencing data from LINK-A-silenced KYSE450 cells.
 (B and C) Western blot analysis of the *in vivo* (B) and *in vitro* (C) interaction between MCM3 and HIF-1 α .
 (D and E) Relative hypoxia response element-driven luciferase activity in the indicated cells. The data are presented as the mean \pm SD values; unpaired Student's t test, ***p < 0.001; n = 3.
 (F and G) Real-time qPCR analysis of HIF-1 α target gene expression in the indicated cells under normoxic and hypoxic conditions. The data are presented as the mean \pm SD values; unpaired Student's t test, *p < 0.05, **p < 0.01, ***p < 0.001, ns = no significant difference; n = 3.
 (H–K) Measurement of the ECAR using a Seahorse assay in the indicated cells. The data are presented as the mean \pm SD values; unpaired Student's t test, **p < 0.01, ***p < 0.001; n = 5.
 (L and M) Relative viability of the indicated cells after DDP treatment for 24 h. Cells were pretreated with licifiguat (YC-1; 100 μ M) or digoxin (100 nM) for 48 h. The data are presented as mean \pm SD values; n = 3.
 (N and O) Measurement of the ECAR using a Seahorse assay in the indicated cells. The data are presented as the mean \pm SD values; unpaired Student's t test, ***p < 0.001; n = 5.
 (P) Relative viability of the indicated cells after DDP treatment for 24 h. The data are presented as the mean \pm SD values; n = 3.

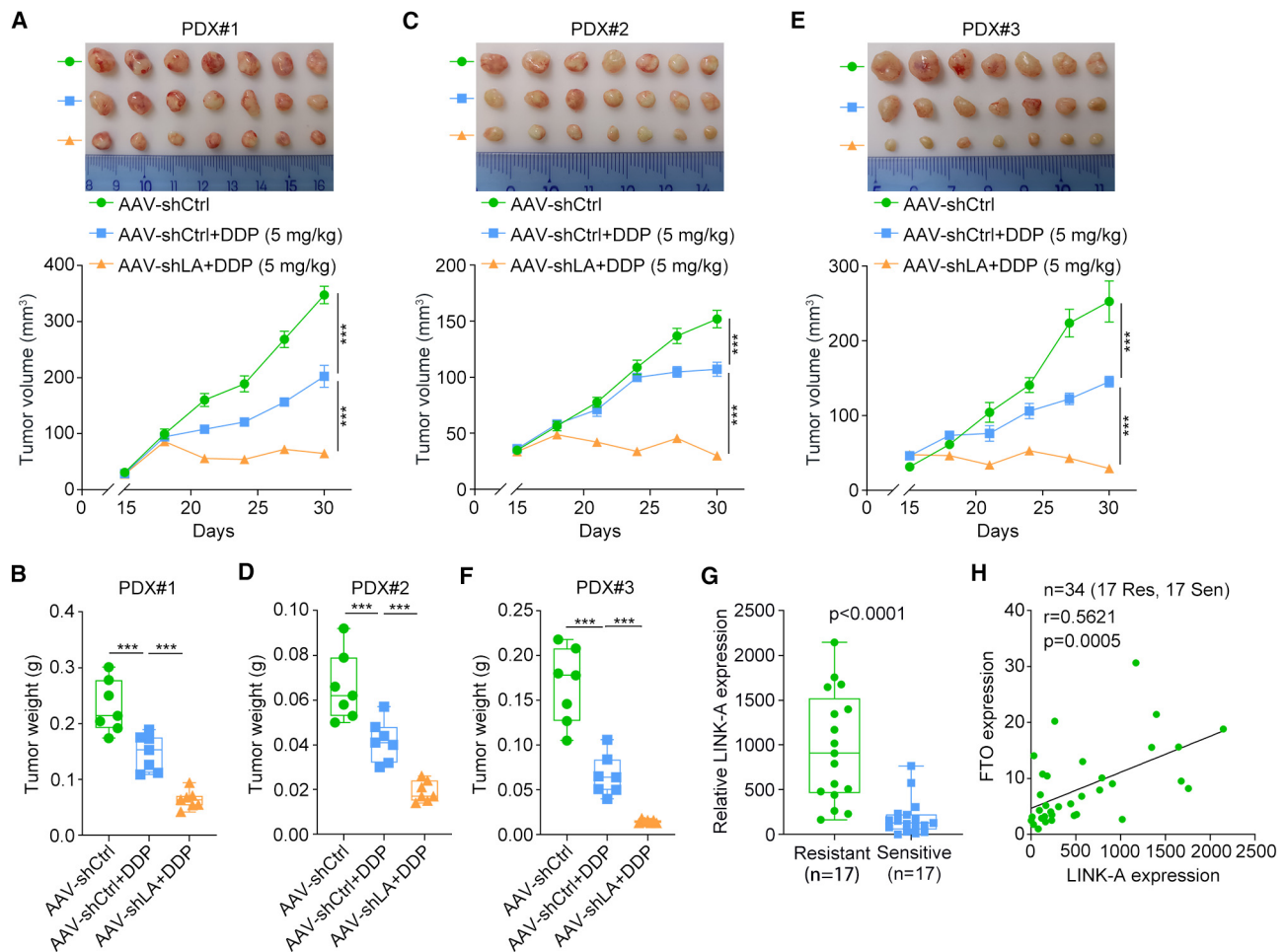


Figure 6. Targeting LINK-A sensitizes ESCC to cytotoxic chemotherapy

(A–F) Tumor growth curves and representative images (A, C, and E) and tumor weights (B, D, and F) in three PDX models of ESCC. Adeno-associated viruses (AAVs) were intratumorally injected every three days for a total of two treatments. The data are presented as the mean \pm SEM values in (A, C, and E). Boxplot representation: from top to bottom—maximum, 75th percentile, median, 25th percentile and minimum values in (B), (D) and (F); unpaired Student's t test, $***p < 0.001$; $n = 7$.

(G) Real-time qPCR analysis of LINK-A expression in baseline samples from patients with ESCC, stratified into groups with either chemosensitivity or chemoresistance. Boxplot representation: from top to bottom—maximum, 75th percentile, median, 25th percentile and minimum values; unpaired Student's t test; $n = 17$ for chemoresistant patients and $n = 17$ for chemosensitive patients.

(H) Correlation analysis between the expression of FTO and LINK-A in ESCC samples. The Spearman correlation coefficient is shown.

samples (Figure 6G). Furthermore, correlation analysis showed that the expression of LINK-A was positively correlated with the expression of FTO in these samples (Figure 6H), further confirming the regulation of LINK-A by FTO during ESCC chemoresistance. Taken together, our findings identify LINK-A as a chief culprit in ESCC chemoresistance and reveal both the potential mechanism of LINK-A-mediated chemoresistance and the stability regulation of LINK-A in ESCC.

DISCUSSION

The m⁶A demethylase FTO has been recognized to play crucial roles in various cancers. However, notably, the roles of FTO in cancer can vary by context. FTO has been demonstrated to function as an oncoprotein in the majority of cancer sub-

types,^{31–37} although it has also been proposed to function as a tumor suppressor in certain cancer subtypes, such as epithelial cancers³⁸ and colorectal cancer.³⁹ In the current study, we identified FTO as a significantly upregulated m⁶A demethylase in patients with ESCC who exhibited chemoresistance compared with those who were chemosensitive. By integrated analysis of these data and our previous data showing that 14 annotated ncRNAs were significantly upregulated in chemoresistant ESCC cell lines compared with the corresponding parental cell lines,²⁷ we identified LINK-A as the lncRNA most significantly stabilized by FTO. As an oncogenic lncRNA, LINK-A has been reported to activate diverse cancer-related pathways in several cancers.^{40–43} Although the oncogenic roles of LINK-A have been proposed, the stability regulation of LINK-A, particularly by m⁶A modification, has not yet been reported. Herein, we

found that FTO stabilizes LINK-A expression via removal of m⁶A and elucidated the oncogenic roles of LINK-A that contribute to cancer cell proliferation and chemoresistance in ESCC.

LINK-A activates HIF-1 α signaling and promotes glycolytic reprogramming and tumorigenesis by facilitating the activation of breast tumor kinase in triple-negative breast cancer.⁴⁰ In addition, LINK-A can activate HIF-1 α in osteosarcoma⁴⁴ and diabetic nephropathy.⁴⁵ Conversely, the MCM3 protein directly binds to the HIF-1 α subunit and synergistically inhibits HIF-1 α transcriptional activity via distinct O₂-dependent mechanisms.³⁰ Here, we identified an important mechanism by which LINK-A indirectly activates HIF-1 α by interacting with MCM3 and releasing HIF-1 α from MCM3-mediated transcriptional repression. Transcriptional activation of HIF-1 α contributes to the metabolic switch from OXPHOS to glycolysis in cancer cells and eventually promotes chemoresistance. Interestingly, we found that the interaction between LINK-A and MCM3 leads to cell-cycle progression and subsequent cell proliferation via another independent mechanism. MCM3 is a member of the MCM family, which was originally identified through a yeast genetic screen.⁴⁶ The MCM2-7 proteins are highly conserved and form a hexameric complex during the G1 phase; this complex is then loaded onto the origin of replication to form a pre-replication complex that is indispensable for the initiation of DNA replication.⁴⁷ CDK1-dependent MCM3 phosphorylation at Ser112 triggers the physical association of MCM3 with the remaining MCM subunits and subsequent chromatin loading of the MCM2-7 complex.²⁹ Our study indicated that LINK-A acts as a protein scaffold to mediate CDK1-dependent phosphorylation of MCM3 at Ser112 and increase the chromatin loading of MCM3, which in turn promotes cell-cycle progression and cell proliferation.

In conclusion, this study reveals the details regarding m⁶A demethylation of LINK-A in ESCC cells. The m⁶A demethylase FTO mediates the stabilization and supports the oncogenic roles of LINK-A. The direct interaction between LINK-A and MCM3 not only increases CDK1-mediated phosphorylation of MCM3 at Ser112, which promotes the assembly and chromatin loading of the MCM2-7 complex and subsequent cell-cycle progression and cell proliferation, but also releases HIF-1 α from MCM3-mediated transcriptional repression, which facilitates tumor metabolic reprogramming and chemoresistance. Collectively, our findings suggest that the FTO/LINK-A/MCM3/HIF-1 α axis is crucial for the progression of ESCC, and this discovery provides a potential therapeutic strategy for targeting LINK-A in patients with ESCC, especially those with high LINK-A expression levels. However, additional preclinical studies are necessary to validate this strategy.

Limitations of the study

While we successfully identified FTO as the specific demethylase responsible for stabilizing LINK-A and promoting its oncogenic functions, certain aspects regarding the precise mechanisms of LINK-A stabilization and degradation remain unclear. Future investigations should focus on identifying the specific enzymes involved in directly stabilizing or degrading LINK-A through m⁶A modification. Additionally, to obtain a comprehensive understanding of the m⁶A modification of LINK-A, it is essential to identify the specific m⁶A reader and writer proteins.

Finally, further preclinical studies are warranted to validate the effectiveness of targeting LINK-A as a strategy to overcome ESCC.

STAR★METHODS

Detailed methods are provided in the online version of this paper and include the following:

- **KEY RESOURCES TABLE**
- **RESOURCE AVAILABILITY**
 - Lead contact
 - Materials availability
 - Data and code availability
- **EXPERIMENTAL MODEL AND STUDY PARTICIPANT DETAILS**
 - Patient samples and ISH
 - Cell lines
 - Animal experiments
- **METHOD DETAILS**
 - Lentivirus production and infection
 - Cell viability assay
 - Live cell analysis
 - Cell cycle analysis
 - Western blot and RT-qPCR analyses
 - m⁶A dot blot assay
 - Chromatin-binding protein isolation
 - RNA pull-down and RIP assays
 - mRNA stability assay
 - Measurement of the RNA synthesis rate
 - Dual-luciferase reporter assay
 - FISH and IF staining
 - Seahorse assays
 - RNA-seq and data analysis
- **QUANTIFICATION AND STATISTICAL ANALYSIS**

SUPPLEMENTAL INFORMATION

Supplemental information can be found online at <https://doi.org/10.1016/j.celrep.2023.113273>.

ACKNOWLEDGMENTS

We thank Dr. Yutaka Shimada (Kyoto University, Kyoto, Japan) for providing the ESCC cell lines. We appreciate Beijing Qinglian Biotech Co., Ltd. (Beijing, China) for performing the MS analyses. Q.L. is supported by a Fellow grant from the Leukemia & Lymphoma Society. X.W. is supported by a National Cancer Center fellowship grant. This study was supported by funding from the National Key R&D Program of China (2021YFC2501000), the Fundamental Research Funds for the Central Universities (3332022135), the National Natural Science Foundation of China (82030089, 82188102, 82172590), the CAMS Innovation Fund for Medical Sciences (2021-I2 M-1-018, 2021-I2 M-1-067), and the Fundamental Research Funds for the Central Universities (3332021091).

AUTHOR CONTRIBUTIONS

Y.N., S.L., Q.L., and X.W. designed the experiments and analyzed the data; Y.N. and S.L. performed most of the experiments; W.C. and P.Z. assisted with the animal studies. Y.L. and R.Z. collected clinical samples; Y.N.

generated the figures and drafted the manuscript; S.L., Y.L., and Z.L. edited the manuscript; Z.L. organized and supervised this study.

DECLARATION OF INTERESTS

The authors declare no competing interests.

INCLUSION AND DIVERSITY

We support inclusive, diverse, and equitable conduct of research.

Received: April 28, 2023

Revised: August 28, 2023

Accepted: September 29, 2023

Published: October 19, 2023

REFERENCES

- Sung, H., Ferlay, J., Siegel, R.L., Laversanne, M., Soerjomataram, I., Jemal, A., and Bray, F. (2021). Global Cancer Statistics 2020: GLOBOCAN Estimates of Incidence and Mortality Worldwide for 36 Cancers in 185 Countries. *CA A Cancer J. Clin.* 71, 209–249. <https://doi.org/10.3322/caac.21660>.
- Thrift, A.P. (2021). Global burden and epidemiology of Barrett oesophagus and oesophageal cancer. *Nat. Rev. Gastroenterol. Hepatol.* 18, 432–443. <https://doi.org/10.1038/s41575-021-00419-3>.
- Fu, Y., Dominissini, D., Rechavi, G., and He, C. (2014). Gene expression regulation mediated through reversible m(6)A RNA methylation. *Nat. Rev. Genet.* 15, 293–306. <https://doi.org/10.1038/nrg3724>.
- Schwartz, S., Mumbach, M.R., Jovanovic, M., Wang, T., Maciag, K., Bushkin, G.G., Mertins, P., Ter-Ovanesyan, D., Habib, N., Cacchiarelli, D., et al. (2014). Perturbation of m6A writers reveals two distinct classes of mRNA methylation at internal and 5' sites. *Cell Rep.* 8, 284–296. <https://doi.org/10.1016/j.celrep.2014.05.048>.
- Cesarini, V., Silvestris, D.A., Tassinari, V., Tomaselli, S., Alon, S., Eisenberg, E., Locatelli, F., and Gallo, A. (2018). ADAR2/miR-589-3p axis controls glioblastoma cell migration/invasion. *Nucleic Acids Res.* 46, 2045–2059. <https://doi.org/10.1093/nar/gkx1257>.
- Luo, H., Zhu, G., Xu, J., Lai, Q., Yan, B., Guo, Y., Fung, T.K., Zeisig, B.B., Cui, Y., Zha, J., et al. (2019). HOTTIP lncRNA Promotes Hematopoietic Stem Cell Self-Renewal Leading to AML-like Disease in Mice. *Cancer Cell* 36, 645–659.e8. <https://doi.org/10.1016/j.ccell.2019.10.011>.
- Li, J., Huang, C., Zou, Y., Ye, J., Yu, J., and Gui, Y. (2020). CircTLK1 promotes the proliferation and metastasis of renal cell carcinoma by sponging miR-136-5p. *Mol. Cancer* 19, 103. <https://doi.org/10.1186/s12943-020-01225-2>.
- Meyer, K.D., and Jaffrey, S.R. (2017). Rethinking m(6)A Readers, Writers, and Erasers. *Annu. Rev. Cell Dev. Biol.* 33, 319–342. <https://doi.org/10.1146/annurev-cellbio-100616-060758>.
- Zaccara, S., Ries, R.J., and Jaffrey, S.R. (2019). Reading, writing and erasing mRNA methylation. *Nat. Rev. Mol. Cell Biol.* 20, 608–624. <https://doi.org/10.1038/s41580-019-0168-5>.
- Patil, D.P., Pickering, B.F., and Jaffrey, S.R. (2018). Reading m(6)A in the Transcriptome: m(6)A-Binding Proteins. *Trends Cell Biol.* 28, 113–127. <https://doi.org/10.1016/j.tcb.2017.10.001>.
- Zheng, G., Dahl, J.A., Niu, Y., Fedorcsak, P., Huang, C.M., Li, C.J., Vågbo, C.B., Shi, Y., Wang, W.L., Song, S.H., et al. (2013). ALKBH5 is a mammalian RNA demethylase that impacts RNA metabolism and mouse fertility. *Mol. Cell* 49, 18–29. <https://doi.org/10.1016/j.molcel.2012.10.015>.
- Jia, G., Fu, Y., Zhao, X., Dai, Q., Zheng, G., Yang, Y., Yi, C., Lindahl, T., Pan, T., Yang, Y.G., and He, C. (2011). N6-methyladenosine in nuclear RNA is a major substrate of the obesity-associated FTO. *Nat. Chem. Biol.* 7, 885–887. <https://doi.org/10.1038/nchembio.687>.
- Weng, H., Huang, H., Wu, H., Qin, X., Zhao, B.S., Dong, L., Shi, H., Skibbe, J., Shen, C., Hu, C., et al. (2018). METTL14 Inhibits Hematopoietic Stem/Progenitor Differentiation and Promotes Leukemogenesis via mRNA m(6)A Modification. *Cell Stem Cell* 22, 191–205.e9. <https://doi.org/10.1016/j.stem.2017.11.016>.
- Yang, X., Zhang, S., He, C., Xue, P., Zhang, L., He, Z., Zang, L., Feng, B., Sun, J., and Zheng, M. (2020). METTL14 suppresses proliferation and metastasis of colorectal cancer by down-regulating oncogenic long non-coding RNA XIST. *Mol. Cancer* 19, 46. <https://doi.org/10.1186/s12943-020-1146-4>.
- DeBerardinis, R.J., Lum, J.J., Hatzivassiliou, G., and Thompson, C.B. (2008). The biology of cancer: metabolic reprogramming fuels cell growth and proliferation. *Cell Metabol.* 7, 11–20. <https://doi.org/10.1016/j.cmet.2007.10.002>.
- Hanahan, D., and Weinberg, R.A. (2011). Hallmarks of cancer: the next generation. *Cell* 144, 646–674. <https://doi.org/10.1016/j.cell.2011.02.013>.
- Hsu, P.P., and Sabatini, D.M. (2008). Cancer cell metabolism: Warburg and beyond. *Cell* 134, 703–707. <https://doi.org/10.1016/j.cell.2008.08.021>.
- Pavlova, N.N., Zhu, J., and Thompson, C.B. (2022). The hallmarks of cancer metabolism: Still emerging. *Cell Metabol.* 34, 355–377. <https://doi.org/10.1016/j.cmet.2022.01.007>.
- Stine, Z.E., Schug, Z.T., Salvino, J.M., and Dang, C.V. (2022). Targeting cancer metabolism in the era of precision oncology. *Nat. Rev. Drug Discov.* 21, 141–162. <https://doi.org/10.1038/s41573-021-00339-6>.
- Chen, F., Chen, J., Yang, L., Liu, J., Zhang, X., Zhang, Y., Tu, Q., Yin, D., Lin, D., Wong, P.P., et al. (2019). Extracellular vesicle-packaged HIF-1 α -stabilizing lncRNA from tumour-associated macrophages regulates aerobic glycolysis of breast cancer cells. *Nat. Cell Biol.* 21, 498–510. <https://doi.org/10.1038/s41556-019-0299-0>.
- Wang, G.L., Jiang, B.H., Rue, E.A., and Semenza, G.L. (1995). Hypoxia-inducible factor 1 is a basic-helix-loop-helix-PAS heterodimer regulated by cellular O₂ tension. *Proc. Natl. Acad. Sci. USA* 92, 5510–5514. <https://doi.org/10.1073/pnas.92.12.5510>.
- Zhao, T., Zhu, Y., Morinibu, A., Kobayashi, M., Shinomiya, K., Itasaka, S., Yoshimura, M., Guo, G., Hiraoka, M., and Harada, H. (2014). HIF-1-mediated metabolic reprogramming reduces ROS levels and facilitates the metastatic colonization of cancers in lungs. *Sci. Rep.* 4, 3793. <https://doi.org/10.1038/srep03793>.
- Denko, N.C. (2008). Hypoxia, HIF1 and glucose metabolism in the solid tumour. *Nat. Rev. Cancer* 8, 705–713. <https://doi.org/10.1038/nrc2468>.
- Ward, P.S., and Thompson, C.B. (2012). Metabolic reprogramming: a cancer hallmark even warburg did not anticipate. *Cancer Cell* 21, 297–308. <https://doi.org/10.1016/j.ccr.2012.02.014>.
- Shigetani, K., Hasegawa, M., Hishiki, T., Naito, Y., Baba, Y., Mikami, S., Matsumoto, K., Mizuno, R., Miyajima, A., Kikuchi, E., et al. (2023). IDH2 stabilizes HIF-1 α -induced metabolic reprogramming and promotes chemoresistance in urothelial cancer. *EMBO J.* 42, e110620. <https://doi.org/10.15252/embj.2022110620>.
- Lan, Q., Liu, P.Y., Bell, J.L., Wang, J.Y., Hüttelmaier, S., Zhang, X.D., Zhang, L., and Liu, T. (2021). The Emerging Roles of RNA m(6)A Methylation and Demethylation as Critical Regulators of Tumorigenesis, Drug Sensitivity, and Resistance. *Cancer Res.* 81, 3431–3440. <https://doi.org/10.1158/0008-5472.CAN-20-4107>.
- Nan, Y., Luo, Q., Wu, X., Liu, S., Zhao, P., Chang, W., Zhou, A., and Liu, Z. (2022). DLGAP1-AS2-Mediated Phosphatidic Acid Synthesis Activates YAP Signaling and Confers Chemoresistance in Squamous Cell Carcinoma. *Cancer Res.* 82, 2887–2903. <https://doi.org/10.1158/0008-5472.CAN-22-0717>.
- Madine, M.A., Khoo, C.Y., Mills, A.D., and Laskey, R.A. (1995). MCM3 complex required for cell cycle regulation of DNA replication in vertebrate cells. *Nature* 375, 421–424. <https://doi.org/10.1038/375421a0>.

29. Lin, D.I., Aggarwal, P., and Diehl, J.A. (2008). Phosphorylation of MCM3 on Ser-112 regulates its incorporation into the MCM2-7 complex. *Proc. Natl. Acad. Sci. USA* *105*, 8079–8084. <https://doi.org/10.1073/pnas.0800077105>.
30. Hubbi, M.E., Luo, W., Baek, J.H., and Semenza, G.L. (2011). MCM proteins are negative regulators of hypoxia-inducible factor 1. *Mol. Cell* *42*, 700–712. <https://doi.org/10.1016/j.molcel.2011.03.029>.
31. Li, Z., Weng, H., Su, R., Weng, X., Zuo, Z., Li, C., Huang, H., Nachtergaele, S., Dong, L., Hu, C., et al. (2017). FTO Plays an Oncogenic Role in Acute Myeloid Leukemia as a N(6)-Methyladenosine RNA Demethylase. *Cancer Cell* *31*, 127–141. <https://doi.org/10.1016/j.ccell.2016.11.017>.
32. Cui, Y., Zhang, C., Ma, S., Li, Z., Wang, W., Li, Y., Ma, Y., Fang, J., Wang, Y., Cao, W., and Guan, F. (2021). RNA m6A demethylase FTO-mediated epigenetic up-regulation of LINC00022 promotes tumorigenesis in esophageal squamous cell carcinoma. *J. Exp. Clin. Cancer Res.* *40*, 294. <https://doi.org/10.1186/s13046-021-02096-1>.
33. Su, R., Dong, L., Li, Y., Gao, M., Han, L., Wunderlich, M., Deng, X., Li, H., Huang, Y., Gao, L., et al. (2020). Targeting FTO Suppresses Cancer Stem Cell Maintenance and Immune Evasion. *Cancer Cell* *38*, 79–96.e11. <https://doi.org/10.1016/j.ccell.2020.04.017>.
34. Cui, Q., Shi, H., Ye, P., Li, L., Qu, Q., Sun, G., Sun, G., Lu, Z., Huang, Y., Yang, C.G., et al. (2017). m(6)A RNA Methylation Regulates the Self-Renewal and Tumorigenesis of Glioblastoma Stem Cells. *Cell Rep.* *18*, 2622–2634. <https://doi.org/10.1016/j.celrep.2017.02.059>.
35. Liu, X., Liu, J., Xiao, W., Zeng, Q., Bo, H., Zhu, Y., Gong, L., He, D., Xing, X., Li, R., et al. (2020). SIRT1 Regulates N(6)-Methyladenosine RNA Modification in Hepatocarcinogenesis by Inducing RANBP2-Dependent FTO SUMOylation. *Hepatology* *72*, 2029–2050. <https://doi.org/10.1002/hep.31222>.
36. Su, R., Dong, L., Li, C., Nachtergaele, S., Wunderlich, M., Qing, Y., Deng, X., Wang, Y., Weng, X., Hu, C., et al. (2018). R-2HG Exhibits Anti-tumor Activity by Targeting FTO/m(6)A/MYC/CEBPA Signaling. *Cell* *172*, 90–105.e23. <https://doi.org/10.1016/j.cell.2017.11.031>.
37. Yang, S., Wei, J., Cui, Y.H., Park, G., Shah, P., Deng, Y., Aplin, A.E., Lu, Z., Hwang, S., He, C., and He, Y.Y. (2019). m(6)A mRNA demethylase FTO regulates melanoma tumorigenicity and response to anti-PD-1 blockade. *Nat. Commun.* *10*, 2782. <https://doi.org/10.1038/s41467-019-10669-0>.
38. Jeschke, J., Collignon, E., Al Wardi, C., Krayem, M., Bizet, M., Jia, Y., Garaud, S., Wimana, Z., Calonne, E., Hassabi, B., et al. (2021). Downregulation of the FTO m(6)A RNA demethylase promotes EMT-mediated progression of epithelial tumors and sensitivity to Wnt inhibitors. *Nat. Can. (Ott.)* *2*, 611–628. <https://doi.org/10.1038/s43018-021-00223-7>.
39. Ruan, D.Y., Li, T., Wang, Y.N., Meng, Q., Li, Y., Yu, K., Wang, M., Lin, J.F., Luo, L.Z., Wang, D.S., et al. (2021). FTO downregulation mediated by hypoxia facilitates colorectal cancer metastasis. *Oncogene* *40*, 5168–5181. <https://doi.org/10.1038/s41388-021-01916-0>.
40. Lin, A., Li, C., Xing, Z., Hu, Q., Liang, K., Han, L., Wang, C., Hawke, D.H., Wang, S., Zhang, Y., et al. (2016). The LINK-A lncRNA activates normoxic HIF1alpha signalling in triple-negative breast cancer. *Nat. Cell Biol.* *18*, 213–224. <https://doi.org/10.1038/ncb3295>.
41. Lin, A., Hu, Q., Li, C., Xing, Z., Ma, G., Wang, C., Li, J., Ye, Y., Yao, J., Liang, K., et al. (2017). The LINK-A lncRNA interacts with PtdIns(3,4,5)P3 to hyperactivate AKT and confer resistance to AKT inhibitors. *Nat. Cell Biol.* *19*, 238–251. <https://doi.org/10.1038/ncb3473>.
42. Ma, J., and Xue, M. (2018). LINK-A lncRNA promotes migration and invasion of ovarian carcinoma cells by activating TGF-beta pathway. *Biosci. Rep.* *38*. <https://doi.org/10.1042/BSR20180936>.
43. Hu, Q., Ye, Y., Chan, L.C., Li, Y., Liang, K., Lin, A., Egranov, S.D., Zhang, Y., Xia, W., Gong, J., et al. (2019). Oncogenic lncRNA downregulates cancer cell antigen presentation and intrinsic tumor suppression. *Nat. Immunol.* *20*, 835–851. <https://doi.org/10.1038/s41590-019-0400-7>.
44. Zhao, B., Liu, K., and Cai, L. (2019). LINK-A lncRNA functions in the metastasis of osteosarcoma by upregulating HIF1alpha. *Oncol. Lett.* *17*, 5005–5011. <https://doi.org/10.3892/ol.2019.10177>.
45. Yang, J., Li, L., Hong, S., Zhou, Z., and Fan, W. (2019). LINK-A lncRNA activates HIF1alpha signaling and inhibits podocyte cell apoptosis in diabetic nephropathy. *Exp. Ther. Med.* *18*, 119–124. <https://doi.org/10.3892/etm.2019.7542>.
46. Maine, G.T., Sinha, P., and Tye, B.K. (1984). Mutants of *S. cerevisiae* defective in the maintenance of minichromosomes. *Genetics* *106*, 365–385. <https://doi.org/10.1093/genetics/106.3.365>.
47. Lei, M., and Tye, B.K. (2001). Initiating DNA synthesis: from recruiting to activating the MCM complex. *J. Cell Sci.* *114*, 1447–1454. <https://doi.org/10.1242/jcs.114.8.1447>.
48. Nan, Y., Luo, Q., Wu, X., Chang, W., Zhao, P., Liu, S., and Liu, Z. (2023). HCP5 prevents ubiquitination-mediated UTP3 degradation to inhibit apoptosis by activating c-Myc transcriptional activity. *Mol. Ther.* *31*, 552–568. <https://doi.org/10.1016/j.ymthe.2022.10.006>.
49. Luo, Q., Wu, X., Zhao, P., Nan, Y., Chang, W., Zhu, X., Su, D., and Liu, Z. (2021). OTUD1 Activates Caspase-Independent and Caspase-Dependent Apoptosis by Promoting AIF Nuclear Translocation and MCL1 Degradation. *Adv. Sci.* *8*, 2002874. <https://doi.org/10.1002/adv.202002874>.

STAR★METHODS

KEY RESOURCES TABLE

REAGENT or RESOURCE	SOURCE	IDENTIFIER
Antibodies		
anti-MCM3	Cell Signaling Technology	#4012; RRID: AB_2235150
anti-CDK1	Cell Signaling Technology	#9116; RRID: AB_2074795
anti-HIF-1 α	Cell Signaling Technology	#36169; RRID: AB_2799095
anti-p-MCM3 (Ser112)	Cell Signaling Technology	#12686; RRID: AB_2797991
anti-FTO	Thermo Scientific	712913; RRID: AB_2815347
anti-MCM2	ABclonal	A1056; RRID: AB_2758102
anti-MCM4	ABclonal	A13513; RRID: AB_2760375
anti-MCM5	ABclonal	A5556; RRID: AB_2766336
anti-MCM6	ABclonal	A1955; RRID: AB_2763981
anti-MCM7	ABclonal	A1138; RRID: AB_2758534
anti-MCM3	Abcam	ab272877
anti-m ⁶ A	Synaptic Systems	202003; RRID: AB_2279214
anti-H3	Abcam	ab1791; RRID: AB_302613
anti-Lamin B1	ABclonal	A1910; RRID: AB_2862592
anti- β -actin	Sigma-Aldrich	A5316; RRID: AB_476743
Bacterial and virus strains		
Escherichia coli strain BL21(DE3)	Biomed	BC201-01
Biological samples		
ESCC tissue array	Servicebio	#G6040
Chemosensitive and chemoresistant ESCC baseline samples	This paper	N/A
Patient-derived xenografts (PDX)	This paper	N/A
Chemicals, peptides, and recombinant proteins		
Polybrene	Sigma-Aldrich	H9268
Puromycin	Sangon Biotech	A610593
G418	MedChemExpress	HY-17561
Actinomycin D	AbMole	M4881
YC-1	MedChemExpress	HY-14927
Digoxin	MedChemExpress	HY-B1049
FB23-2	MedChemExpress	HY-127103
Critical commercial assays		
Duolink <i>In Situ</i> Red Starter Kit	Sigma-Aldrich	DUO92101
Cell Mito Stress Test Kit	Agilent Technologies	103015
Glycolysis Stress Test Kit	Agilent Technologies	103020
FISH Kit	RiboBio	C10910
Deposited data		
RNA-seq	This paper	GEO: GSE224079
Mass spectrometry	This paper	PRIDE: PXD045414
Experimental models: Cell lines		
Human: ESCC cell lines	Dr. Yutaka Shimada (Kyoto University, Kyoto, Japan)	N/A
Human: 293T	ATCC	CRL-3216; RRID: CVCL_0063
Human: Het-1A	ATCC	CRL-2692; RRID: CVCL_3702

(Continued on next page)

Continued

REAGENT or RESOURCE	SOURCE	IDENTIFIER
Experimental models: Organisms/strains		
Mouse: BALB/cA-nu	HFK Bioscience	N/A
Mouse: NOD-Prkdc ^{scid} -Il2rg ^{em1} IDMO (NPI)	IDMO	N/A
Oligonucleotides		
See Table S3 for oligonucleotide sequences for shRNA and sgRNA	This paper	N/A
See Table S4 for oligonucleotide sequences for RT-qPCR primers	This paper	N/A
Recombinant DNA		
Plasmid: psPAX2	Gift from Didier Trono	Addgene plasmid #12260; RRID: Addgene_12260
Plasmid: pMD2.G	Gift from Didier Trono	Addgene plasmid #12259; RRID: Addgene_12259
Plasmid: pSIH1-puro	This paper	N/A
Plasmid: pLVX-IRES-neo	This paper	N/A
Plasmid: pGEX-6P-1	This paper	N/A
Software and algorithms		
GraphPad Prism version 8.3.0	GraphPad Software	https://www.graphpad.com/

RESOURCE AVAILABILITY

Lead contact

Further information and requests for resources and reagents should be directed to and will be fulfilled by the lead contact, Zhihua Liu (liuzh@cicams.ac.cn).

Materials availability

This study did not generate new unique reagents.

Data and code availability

All data reported in this paper will be shared by the [lead contact](#) upon request. The RNA-seq data have been deposited in the Gene Expression Omnibus database under accession number GSE224079. The mass spectrometry proteomics data have been deposited in the ProteomeXchange datasets under accession number PXD045414.

This paper does not report the original code.

Any additional information required to reanalyze the data reported in this paper is available from the [lead contact](#) upon request.

EXPERIMENTAL MODEL AND STUDY PARTICIPANT DETAILS

Patient samples and ISH

This study was approved by the Research Ethics Committee of the Chinese Academy of Medical Sciences Cancer Hospital. A total of 34 baseline samples from patients treated with neoadjuvant chemotherapy were collected from the Cancer Hospital Chinese Academy of Medical Sciences. Written informed consent was obtained from all patients. The detailed information of the 34 patients in [Table S1](#). Human tissue microarray slides from patients with ESCC were obtained from Servicebio (#G6040; Servicebio, Wuhan, China), including samples from 216 individuals diagnosed with ESCC, with normal paired tissues available for 169 of these individuals with ESCC. The detailed information of this cohort in [Table S2](#). RNA ISH was performed as previously described.²⁷ The sequences of the probes used for ISH were as follows (5' to 3'): Probe #1, CACTAGGGTGGAACCTCAGGAAGTTGATGACATTTGTAGC; Probe #2, GCTTATAATTCTTAATTACTAACAATGCTGGTATGAAA; and Probe #3, GACTCGCTCTGGCCGTATGTAATGATGTCTGTGGCT ACAT.

Cell lines

The human ESCC cell lines were kindly provided by Dr. Yutaka Shimada (Kyoto University, Kyoto, Japan). The 293T cell line was purchased from the American Type Culture Collection (ATCC, VA, USA). ESCC cells were cultured in RPMI-1640 medium supplemented with 10% fetal bovine serum (FBS), and 293T cells were cultured in Dulbecco's modified Eagle's medium (DMEM) supplemented with

10% FBS. All cells were cultured under aseptic conditions at 37°C in 5% CO₂ and passaged with 0.25% trypsin. All cell lines were routinely verified using short tandem repeat DNA fingerprinting and were tested for Mycoplasma contamination using a MycoBlue Mycoplasma Detector (D101; Vazyme Biotech, Nanjing, China) before use in any experiments.

Animal experiments

All animal protocols were approved by the Animal Care and Use Committee of the Chinese Academy of Medical Sciences Cancer Hospital. Cell-derived xenografts and PDXs were established as previously described.⁴⁸ The 6-week-old male BALB/c nude mice (HFK Bioscience, Beijing, China) were used for subcutaneous xenografts, and 6-week-old male NOD-Prkdc^{scid}-Il2rg^{em11D^{MO}} (NPI) mice (IDMO, Beijing, China) were used as hosts for PDX tumors. The saline or DDP (5 mg/kg) treatment approximately 1–2 weeks after xenografting (the tumor volumes are approximately 75–100 mm³), administering it through intraperitoneal injection and continuing until the point of sacrifice. Mice bearing PDXs were administered two intratumoral injections, at 3-day intervals, with AAV expressing shCtrl or AAV expressing shLINK-A (2.5 × 10¹¹ vg/mouse) produced by ViGene Biosciences (Jinan, China). The tumor volume was calculated as follows: 0.52 × length × width.² The combination index (CI) was calculated as follows: CI=(E1/E2)/(C1/C2), where E1 is the mean tumor volume or weight in the experimental arm (e.g., gene overexpression or knockdown arm) with drug treatment, E2 is the mean tumor volume or weight in the experimental arm with vehicle treatment, C1 is the mean tumor volume or weight in the control arm (e.g., empty vector or control shRNA arm) with drug treatment, and C2 is the mean tumor volume or weight in the control arm with vehicle treatment. CI < 1, = 1, and >1 indicate synergistic, additive, and antagonistic effects, respectively.

METHOD DETAILS

Lentivirus production and infection

The full-length cDNA of LINK-A was synthesized using PCR amplification and subsequently inserted into the pLVX-IRES-neo vector (#632184; Clontech, CA, USA). The full-length cDNA of MCM3 was inserted into the PEZ-LV105 vector (M0227; GeneCopoeia, Guangzhou, China). The shRNA sequences were inserted into the pSIH1-puro vector (#26597; Addgene, MA, USA). The single-guide RNA (sgRNA) sequences were inserted into the LentiCRISPR v2 (#52961; Addgene) backbone. For construction of the MCM3^{S112A} mutant plasmid, the plasmid containing the MCM3 ORF was used as the template for PCR. The first round of PCR was performed with two pairs of primers containing the mutation site, and the second round of PCR was performed with primers targeting both ends of the product from the first round of PCR. Finally, the obtained fragment was ligated into the vector via restriction endonuclease digestion, and the mutation site was verified by Sanger sequencing. The sequences of the PCR primers used for mutant construction were as follows (5' to 3'): F1, CGGAATTCGCCACCATGGCGGGTACCGTGCT; R1, GCTCTAGATCATTGTCATCGTCGTCCTTGTAATCCTAGATGAGGAAGATGATGC; F2, AAGCACGTCGCCCGCGGAC; and R2, GTCCGCGGGGCGACGTGCTT. Transfection was performed using Hieff *trans* Liposomal Transfection Reagent (40802; Yeasen, Shanghai, China) according to the manufacturer's protocol. Lentiviruses were produced in 293T cells with a second-generation packaging system containing psPAX2 (#12260; Addgene) and pMD2.G (#12259; Addgene). Cells were subjected to two rounds of lentiviral transduction in the presence of 8 μg/mL polybrene (H9268; Sigma-Aldrich, MO, USA) within a 48-h period, and stable transductants were then selected by culture with 1 μg/mL puromycin (A610593; Sangon Biotech, Shanghai, China) or 200 μg/mL G418 (HY-17561; MedChemExpress, NJ, USA) for 7 days. The shRNA and sgRNA sequences are listed in Table S3.

Cell viability assay

The cell proliferation rate and cell viability were assessed as previously described.²⁷ For experiments with the HIF-1α inhibitors (YC-1 (HY-14927; MedChemExpress) and digoxin (HY-B1049; MedChemExpress)), cells were treated with the agents at the corresponding concentrations for 48 h before seeding into 96-well plates. Cell Counting Kit-8 reagent (CK04; Dojindo Laboratories, Kumamoto, Japan) was used to assess the cell proliferation rate and cell viability after DDP treatment according to the manufacturer's instructions.

Live cell analysis

An InCuCyte Live Cell Imaging System (Essen Bioscience, Hertfordshire, UK) was used for live cell imaging. Cells were seeded in 96-well plates, and drugs were added after cell adhesion. The plates were placed in the InCuCyte system, and snapshots of two regions per well were acquired at 3-h intervals over a 72-h period. Cell confluence was quantified with the accompanying commercial software.

Cell cycle analysis

Cell cycle analysis was performed using a Cell Cycle Assay Kit (C543; Dojindo Laboratories) according to the manufacturer's instructions. The cell cycle distribution was analyzed using a flow cytometer.

Western blot and RT-qPCR analyses

Western blot analysis was performed as previously described.⁴⁹ In brief, ESCC cells were lysed with RIPA buffer (CW2333; CWBIO, Beijing, China) containing protease inhibitor cocktail tablets (04693132001; Roche, Prague, Czech Republic). Protein concentrations

were determined using a BCA assay kit (23225; Thermo Scientific, MA, USA). The following antibodies were used for Western blot analysis: anti-MCM3 (#4012; Cell Signaling Technology, MA, USA; 1:1000), anti-CDK1 (#9116; Cell Signaling Technology; 1:1000), anti-HIF-1 α (#36169; Cell Signaling Technology; 1:1000), anti-phospho-MCM3 (Ser112) (#12686; Cell Signaling Technology; 1:1000), anti-FTO (712913; Thermo Scientific; 1:1000), anti-MCM2 (A1056; ABclonal, Wuhan, China; 1:1000), anti-MCM4 (A13513; ABclonal; 1:1000), anti-MCM5 (A5556; ABclonal; 1:2000), anti-MCM6 (A1955; ABclonal; 1:1000), anti-MCM7 (A1138; ABclonal; 1:1000), anti-H3 (ab1791; Abcam, MA, USA; 1:1000), anti-Lamin B1 (A1910; ABclonal; 1:2000), and anti- β -actin (A5316; Sigma-Aldrich; 1:4000).

To obtain purified MCM3, CDK1 and HIF-1 α proteins, the pGEX-6P-1-MCM3, pGEX-6P-1-HIF-1 α and pGEX-6P-1 plasmids were transformed separately into *Escherichia coli* BL21 (DE3) cells (BC201-01, Biomed, Beijing, China). Protein expression was induced by overnight incubation with 0.5 mM isopropyl- β -D-thiogalactoside (IPTG) at 25°C. Finally, proteins were purified on GST purification columns (16107; Thermo Scientific) according to the manufacturer's instructions. Purified proteins were concentrated by filtering through Amicon Ultra0.5 Centrifugal Filter Units (UFC503008; Millipore, MA, USA). To explore the direct protein-RNA interactions *in vitro*, the purified MCM3 protein was first incubated with a magnetic bead-conjugated antibody. After incubation, the protein sample was divided into two aliquots, and 2 μ g of the *in vitro*-transcribed LINK-A sense or antisense strand was then added separately. The same amount of purified CDK1 or HIF-1 α protein was added simultaneously. After incubation for 12 h at 4°C, the immunoprecipitated protein complexes were washed 4 times with Tris-buffered saline supplemented with 0.5% Triton X-100 and analyzed by Western blotting.

For the IP assay, an anti-MCM3 antibody (ab272877; Abcam; 1:100) was incubated with protein A/G magnetic beads (88803; Thermo Scientific) at 4°C for 6–8 h. Cells were lysed in IP lysis buffer (P0013; Beyotime Biotechnology, Shanghai, China) containing protease inhibitor cocktail tablets (04693132001; Roche). Equal amounts of lysates were incubated with the magnetic bead-conjugated antibodies overnight at 4°C. Then, the immunoprecipitated proteins were washed 4 times with Tris-buffered saline supplemented with 0.5% Triton X-100 and analyzed by Western blotting.

RNA preparation and RT-qPCR were performed according to previously described methods.²⁷ The sequences of the primers used for RT-qPCR are listed in Table S4.

m⁶A dot blot assay

RNA samples were diluted to the same concentration in RNase-free water and then denatured by incubation at 95°C for 3 min. Two microliters of each RNA sample was then dropped directly onto a Hybond-N+ membrane (RPN119B; GE Healthcare Life Sciences, Uppsala, Sweden). The RNA samples were crosslinked onto the membrane by dehydration at 37°C for 30 min. The membrane was washed twice in TBST and blocked with 5% nonfat milk for 1 h at room temperature. The membrane was then incubated first with an anti-m⁶A antibody (202003; Synaptic Systems, Goettingen, Germany; 1:500) at 4°C overnight and then incubated with HRP-conjugated goat anti-rabbit IgG. Immunoreactions were visualized with ECL Western blotting solution. Finally, the membrane was stained with 0.02% methylene blue to verify equal loading.

Chromatin-binding protein isolation

Chromatin-binding proteins were isolated from cultured cells using a subcellular protein isolation kit (78840; Thermo Scientific) according to the manufacturer's instructions. In brief, two million ESCC cells were collected, and proteins in the cell fractions were obtained by successively adding lysates of the different cell fractions and performing differential centrifugation. The final protein lysate containing the chromatin-binding fraction was obtained, and the protein concentration was determined with a BCA kit.

RNA pull-down and RIP assays

RNA pull-down and RIP assays were performed as previously reported.²⁷ Negative control IgG (#2729; Cell Signaling Technology) and anti-MCM3 (ab272877; Abcam; 1:100) and anti-m⁶A (202003; Synaptic Systems; 1:100) antibodies were used in the RIP assay. Proteins precipitated by the LINK-A sense and antisense strands were identified using a gel-based LC-MS/MS approach (Beijing Qinglian Biotech Co., Ltd., Beijing, China). The data were analyzed using MaxQuant software (version 1.5.3.30), and the spectra were searched against the UniProtKB/Swiss-Prot human database. Proteins specifically associated with the LINK-A sense strand in YES2 and KYSE450 cell lines are listed in Table S5.

mRNA stability assay

Cells were treated with 5 μ g/mL actinomycin D (M4881; AbMole, TX, USA) to block *de novo* RNA synthesis. Total RNA was collected at different time points, and the expression of LINK-A was measured by RT-qPCR. The half-life of RNA was determined by comparing the RNA level at each time point with the RNA level at time 0 with normalization to the GAPDH RNA level.

Measurement of the RNA synthesis rate

Cell samples were labeled with ethynyl uridine (EU) by incubation in 0.25 mM EU-supplemented growth medium for either 4 h or 5 h, and the relative RNA synthesis rate was calculated over a 5-h period with a 4-h pulse duration. After incubation, 90% ethanol was added to fix the cells, and 0.5% Triton X-100 was then used to permeabilize the cells. The cells were treated with click reaction solution (0.25 mM biotin-azide, 0.3 mM CuSO₄, 0.6 mM tris(benzyltriazolylmethyl)amine (THPTA), 1 mM aminoguanidine, and 5 mM

sodium L-ascorbate) and lysed with lysis buffer (20 mM Tris-HCl (pH 7.5), 500 mM LiCl, 1 mM EDTA (pH 8.0), 0.5% lithium dodecylsulfate (LiDS), and 5 mM dithiothreitol (DTT)) for 30 min on ice. Then, 100 μ L of streptavidin-conjugated magnetic beads was added to each dish, the dishes were incubated for 2 h at 4°C, and the cells were washed 6 times with lysis buffer. Finally, RNA elution buffer (10 mM EDTA (pH 8.2) and 95% formamide) was added, and the dishes were incubated at 90°C for 5 min. RNA extraction and RT-qPCR were performed according to the method described above.

Dual-luciferase reporter assay

To detect transcriptional activation of HREs, the HRE-luciferase plasmid (#26731; Addgene) was transfected into cells with LINK-A interference. After 48 h, luciferase activity was measured using a Dual-Luciferase Reporter Assay System (E1960; Promega, WI, USA). Luciferase activity was calculated as the ratio of firefly luciferase activity to Renilla luciferase activity.

FISH and IF staining

Cells were seeded into a μ -Slide VI (80666; ibidi, Martinsried, Germany) at 60% confluence. After adherence, the cells were fixed with 4% paraformaldehyde and permeabilized with 0.5% Triton X-100 prior to blocking with 5% bovine serum albumin. FISH was performed using a lncRNA FISH Kit (C10910; RiboBio, Guangzhou, China). Hybridization was carried out overnight in a humidified chamber at 37°C in the dark. After probe binding, the cells were incubated with primary antibodies overnight at 4°C. Proteins were visualized by incubation with Alexa Fluor 488-conjugated anti-rabbit IgG (#4412; Cell Signaling Technology) or Alexa Fluor 594-conjugated anti-rabbit IgG (#8890; Cell Signaling Technology), and nuclei were stained with Hoechst 33342 (H21492; Thermo Scientific) for 15 min at room temperature. Finally, images were acquired by confocal microscopy. PLA was performed using a Duolink *In Situ* Red Starter Kit (DUO92101; Sigma-Aldrich) following the manufacturer's protocol. The negative control involves the incubation of only the secondary antibody without the primary antibody, while keeping all other conditions consistent with the experimental group.

Seahorse assays

The OXPHOS and glycolytic capacities were measured with a Seahorse XF96 Extracellular Flux Analyzer (Agilent Technologies, CA, USA). A Cell Mito Stress Test Kit (103015; Agilent Technologies) and Glycolysis Stress Test Kit (103020; Agilent Technologies) were used to measure the OCR and ECAR, respectively. Specifically, 1×10^4 KYSE410 or 1.2×10^4 KYSE450 cells were seeded into Seahorse XF96 Cell Culture Microplates (101085; Agilent Technologies). The ECAR was measured as follows. After cell adherence, the cell medium was replaced with XF RPMI Base Medium (103575; Agilent Technologies) containing 2 mM glutamate. After calibration was completed, glucose (final concentration: 10 μ M), oligomycin (final concentration: 1 μ M) and 2-deoxy-D-glucose (2-DG; final concentration: 50 μ M) were added successively. The OCR was measured as follows. After cell adherence, the cell medium was replaced with XF RPMI Base Medium (103575; Agilent Technologies) containing 2 mM glutamate, 1 mM sodium pyruvate and 10 mM glucose. After calibration was completed, oligomycin (final concentration: 1.5 μ M), carbonyl cyanide 4-(trifluoromethoxy)phenylhydrazone (FCCP; final concentration: 1 μ M), and rotenone/antimycin A (Rot/AA; final concentration: 0.5 μ M) were added successively. Wave software (Agilent Technologies) was used to analyze the raw data, with biological triplicates established for each group.

RNA-seq and data analysis

RNA-seq and data analysis were performed by Shanghai Applied Protein Technology Co., Ltd (Shanghai, China). Three replicates were prepared for each group from independent cell cultures. Paired-end libraries were prepared using an NEBNext Ultra RNA Library Prep Kit for Illumina (New England Biolabs, MA, USA) following the manufacturer's instructions, and sequencing was performed using the Illumina NovaSeq 6000 platform. A fold change of > 2 and p value of < 0.05 were set as the criteria for identifying significantly differentially expressed genes.

QUANTIFICATION AND STATISTICAL ANALYSIS

Statistical analysis was performed using GraphPad Prism 8.3.0 (GraphPad Software, CA, USA). Unpaired or paired Student's *t* test, two-way ANOVA, and the Kaplan–Meier method were used for comparisons between two groups, comparisons among multiple groups, and survival analysis, respectively. Statistical significance was assumed for p values ≤ 0.05 , and results from at least three biologically independent experiments with similar results are reported. The data are presented as the mean \pm s.e.m. or mean \pm s.d. values.